ELSEVIER

Thin Solid Films 323 (1998) 126–135

thin solid films

Growth and characterization of IV–VI semiconductor heterostructures on (100) BaF_2

I-Na Chao [a,*], Patrick J. McCann [a], Wei-Li Yuan [b], Edgar A. O'Rear [b], Shu Yuan [c]

[a] School of Electrical and Computer Engineering, University of Oklahoma, Norman, OK 73109, USA
[b] School of Chemical Engineering, University of Oklahoma, Norman, OK 73109, USA
[c] Department of Electronic Materials Engineering, Research School of Physical Sciences and Engineering, The Australian National University, Canberra, ACT 0200, Australia

Received 30 September 1997; accepted 20 November 1997

Abstract

Techniques for growing p-$PbSe_{0.78}Te_{0.22}$/n-$Pb_{1-x}Sn_xSe_{1-y}Te_y$/n-$PbSe_{0.78}Te_{0.22}$ double heterostructures (x up to 0.2 in the liquid growth solution) on (100) BaF_2 substrates by liquid phase epitaxy (LPE) are described. Inclusion-free epilayers and good wipeoffs have been consistently achieved using these techniques. Surface morphology of the epilayers is investigated using Nomarski microscopy and atomic force microscopy (AFM). Fourier transform infrared (FTIR) transmission measurements show optical absorption edge energies vary monotonically with tin content and with temperature at an average rate of 0.41 meV per degree in the temperature range of 300 K to 130 K. Tunable diode lasers (TDLs) fabricated from these structures are expected to span a spectral range of 5–7 μm for $x = 5\%$ and 6–9 μm for $x = 12\%$ in this temperature range. © 1998 Elsevier Science S.A. All rights reserved.

Keywords: Liquid phase epitaxy; Heterostructures; Epilayers; Wipeoffs

1. Introduction

The IV–VI semiconductor materials system, due to its direct and temperature sensitive bandgap, is suitable for fabricating infrared (IR) lasers that can be fine tuned by temperature or current. The bandgap energy of IV–VI compounds can be tailored to cover regions of the IR spectrum from 3 μm to over 30 μm by adjusting alloy compositions. For example, $PbSe/Pb_{1-x}Sn_xSe_{1-y}Te_y/PbSe$ double heterostructure lasers with various tin contents span a spectrum of 7.4–20.2 μm at 20 K [1]. Tuned by temperature, $Pb_{0.912}Sn_{0.088}Se_{1-y}Te_y$ shows an emission range from 19.3 μm at 20 K to 10.4 μm at 130 K. Fig. 1 shows the composition-dependent bandgap energy vs. lattice parameter plot at 77 K for this materials system. Since many molecules have strong absorption bands in the mid- to far-IR, IV–VI semiconductor lasers are useful as light sources in high-resolution IR spectroscopy applications such as air pollution monitoring [2] and medical diagnostics [3].

Commercially available IV–VI semiconductor lasers are grown on PbTe or PbSe substrates and require liquid nitrogen cooling for continuous wave (CW) operation due to the poor thermal conductivity of the substrate materials. PbSe-based tunable diode lasers (TDLs) using liquid phase epitaxy (LPE)-grown PbSnSeTe as the active layer have a maximum CW operation temperature of 130 K [1]. PbTe-based TDLs using molecular beam epitaxy (MBE)-grown PbTe as the active layer in the $Pb_{1-x}Eu_xSe_{1-y}Te_y/PbTe$ separate confinement buried heterostructures have reached a CW operation temperature of 223 K [4]. Presently, this is the highest CW operation temperature for any semiconductor mid-IR laser including quantum cascade lasers [5].

An alternate substrate material, single crystalline BaF_2, has been used for growing IV–VI semiconductors by LPE [6–10]. Based on Hall effect characterization, these native n-type alloys become p-type when doped with thallium acceptor impurities at concentrations greater than 1.4 at.% in the liquid growth solution [9]. Fourier transform infrared (FTIR) transmission studies of the LPE-grown

* Corresponding author. University of Oklahoma, School of Electrical Eng. and Computer Science, 202 W. Boyd, Room 219, Norman, OK 73019, USA. Tel.: +1-405-325-4721; fax: +1-405-325-7066; e-mail: ichao@mailhost.ecn.uoknor.edu.

0040-6090/98/$19.00 © 1998 Elsevier Science S.A. All rights reserved.

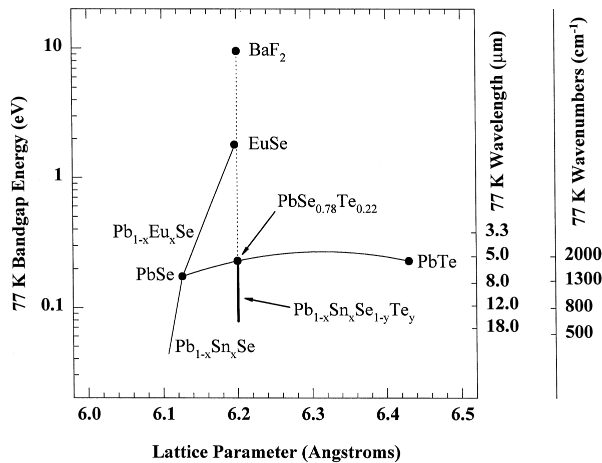

Fig. 1. Lattice matching plot showing bandgap energies at 77 K vs. lattice parameters for different IV–VI semiconductors. Notice that alloying with tin decreases the bandgap while alloying with europium increases the bandgap.

$PbSe_{0.78}Te_{0.22}$ and $Pb_{0.95}Sn_{0.05}Se_{0.80}Te_{0.20}$ (Sn ~ 5%) single layers show that optical absorption edge energies increase with temperature at a rate of 0.46 meV K^{-1} above 100 K, and strong photoluminescence from these epilayers using low argon laser pump power indicates that these materials are suitable for laser fabrication [11]. Using ternary $PbSe_{0.78}Te_{0.22}$ as the cladding layer and quaternary $Pb_{0.95}Sn_{0.05}Se_{0.80}Te_{0.20}$ as the active layer, diode lasers fabricated from these materials are expected to have a tuning range from 10.3 μm (970 cm^{-1}) to 6.4 μm (1560 cm^{-1}) when heated from 77 to 275 K. The technology of growing IV–VI semiconductors on BaF_2 enables the development of a new laser fabrication method that should increase CW operating temperatures to greater than 260 K [12–14]. By improving active region heat dissipation IV–VI TDL fabricated by this new method can thus be cooled thermoelectrically, eliminating the use of liquid nitrogen. In this paper we report the growth and characterization of IV–VI semiconductor laser structures that can enable such device fabrication. Techniques for growing heterostructures such as p-$PbSe_{0.78}Te_{0.22}$/n-$Pb_{1-x}Sn_xSe_{1-y}Te_y$/p-$PbSe_{0.78}Te_{0.22}$ (x up to 0.2 in the liquid growth solution) double heterostructures on (100) BaF_2 substrates, shown in Fig. 2, are discussed. Growth morphology characterization using optical Nomarski microscopy and atomic force microscopy (AFM), and optical transmission studies using FTIR are presented.

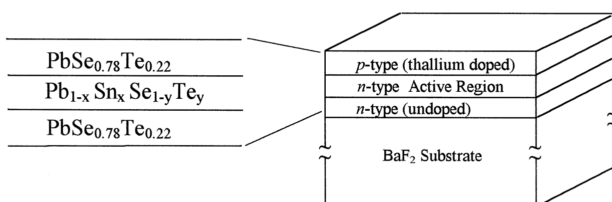

Fig. 2. Lattice-matched IV–VI semiconductor double heterostructures grown by LPE on (100) BaF_2 substrates.

2. Liquid phase epitaxy

In LPE a supersaturated liquid growth solution is cooled slowly from a temperature well below the melting point of the desired semiconductor so that the semiconductor recrystallizes from the solution onto the substrate. The amount of supersaturation is the driving force for nucleation and a concentration gradient in the liquid/solid interface at phase equilibria enables continuity of growth as governed by the laws of thermodynamics. Using known phase equilibria data [15] lattice-matched $PbSe_{0.78}Te_{0.22}$, and $Pb_{1-x}Sn_xSe_{1-y}Te_y$ epilayers have previously been grown on (100)-oriented BaF_2 ($a_o = 6.200$ Å) substrates [7–9]. Lattice matching is accomplished by controlling tellurium concentration in the liquid growth solution. The keys to successful IV–VI epitaxy directly on BaF_2 by LPE are the correct growth initiation temperature in the range of 610°C to 660°C and chalcogen partial pressure over BaF_2 growth surface. There exists a strong correlation between the growth initiation temperature and the substrate surface reaction in which selenium vapor reacts with BaF_2 to form a barium selenium binary compound which serves as a catalyst for nucleation [16]. Sufficient chalcogen partial pressure is accomplished by trapping chalcogen vapor from the growth solution in a properly designed graphite boat [17].

3. Experimental apparatus

The recently designed graphite boat discussed in Ref. [17] was used for all 44 growth experiments. The boat is housed inside a LPE furnace [15] which is normally flushed with 99.9999% pure hydrogen gas during growth to prevent unwanted oxidation of the growth materials. Fig. 3 shows a schematic of the boat which contains four top-loading growth wells in the upper portion of the boat. Sandwiched between the upper portion and the lower portion of the boat is a horizontal-moving graphite slider. The 1-cm^2 BaF_2 substrate is housed in a slightly larger

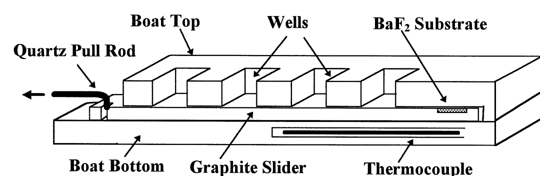

Fig. 3. Schematic of the LPE boat used in this study. The BaF_2 substrate is placed in a recess (substrate pocket). The boat was designed [18] so that all three portions, the boat top, the slider, and the boat bottom, fit intimately. The boat is sealed in a furnace, and the temperature is monitored by a type K thermocouple.

substrate pocket on the slider. The top surface of the slider comes in intimate contact with the bottom of the upper portion of the boat and serves as the floor for the growth wells. The substrate pocket can be positioned under a designated growth well by hand pulling using an attached quartz rod. Substrate pockets of 20, 36, and 62 mils in depth have been milled on various locations on the slider and used for different growth experiments. Completely overlapping multiple layers can be grown by positioning the substrate in alignment with the wells. Partially overlapping layers can be grown by progressively misaligning the substrate with a subsequent well. A structure thus grown allows investigation of the growth results of each layer.

Although the boat was designed to have a tight fit, it was observed that rotation of the quartz pulling rod could tilt the boat and raise the boat top during slider pulling. This situation, in addition to allowing chalcogen vapor to escape, resulted in spilling of growth solutions and poor growth solution wipeoffs. A boat locking system was therefore installed to further secure the closure between the boat top and the slider during slider pulling.

4. Substrate preparation

BaF_2 slabs 1 $cm^2 \times \sim 1$ mm thick were obtained by cutting (100) oriented BaF_2 ingots with a diamond saw. The saw damage was removed by hand polishing the BaF_2 growth surface with 5 or 3 μm alumina grits on a quartz polishing plate. A final polishing step was performed using 0.5 μm grits on a polishing cloth. Following polishing, the BaF_2 growth surface was etched using two methods to remove polishing damage and to provide step sites for nucleation. Since BaF_2 is water soluble, the first technique involved submersion in magnetically stirred deionized (DI) water for ~ 45 min and was used for the first 28 experimental runs. The second technique was conducted using a chemical–mechanical polishing process and was used for the remaining 14 runs. In this method, the BaF_2 growth surface was hand polished less than 30 s on a flat polishing cloth wetted first with DI water then with a 33% hydrochloric (HCl) acid solution. The etched surface was immediately rinsed with methanol to remove the acid and then blown dry with purified nitrogen. Just before commencement of a growth experiment, the BaF_2 growth surface was given a final rinse with DI water for the first method or the HCl acid solution for the second method.

It is important that all scratches on BaF_2 growth surface be removed by polishing and etching. A properly prepared BaF_2 growth surface shows shallow etch pits ~ 0.5 μm deep and (100) facets when observed under an optical microscope. All scratches due to mechanical polishing should also exhibit the (100) facets. Unetched scratches usually result in inclusion (metal precipitation) on the epilayer along the lines of the scratches. Deeper scratches presented a particular problem for the chemical–mechanical etching procedure. These scratches could not be removed by the fast acting acid solution without over etching thus damaging the growth surface.

Based on results of previous LPE growth experiments, the thickness of BaF_2 slabs after polishing should be less than, by within 1 mil (~ 25 μm), the depth of the substrate pocket. The clearance, the distance between the growth surface and the surface of the slider, was measured following etching at the four corners of BaF_2 growth surface using a focusing method under a Nomarski optical microscope. Graphite spacers with specific thickness, if needed, were placed under the BaF_2 substrate to help achieve the desired clearance. Excessive substrate clearance usually resulted in poor growth and poor growth solution wipeoff. On the other hand, BaF_2 protruding above the slider by as little as 2 μm at one corner of BaF_2 growth surface usually resulted in scratches on the epitaxial layer surface caused by the upper portion of the boat during slider pulling. Poorer growth or inclusions were almost always present on a subsequently grown layer where the damage occurred.

Not all growth experiments started with good BaF_2 substrates. For example, among double layer growth experiments (runs #29 to #37) only runs #33 and #36 used good substrates. Runs #33 and #36 produced essentially inclusion-free, smooth epilayers while others using poorer substrates that were improperly polished, etched, or had too much clearance (> 40 μm) resulted in epilayers of lesser quality and poor growth solution wipeoffs.

5. Growth solution and nucleation temperature

The liquid growth solution $(Pb_{1-x}Sn_x)_{1-z}(Se_{1-y}Te_y)_z$ with x ranging from 0.05 to 0.4 were obtained by dissolving small amounts of polycrystalline PbTe and PbSe (both of which have high melting points) in large amounts of Pb and Sn (both of which have low melting points). Thallium

Table 1
Growth parameters of growth solutions for a LPE-grown double heterostructure p-PbSeTe/n-PbSnSeTe/n-PbSeTe

Epilayer	Te content y (%)	Chalcogen content z (%)	Nucleation temperature (°C)	Growth temperature (°C)
1st	60.03	3.20	626	628
2nd	59.68	1.00	510	511
3rd	59.93	0.50	466	467

Sn = 12.03%, Tl = 3.00% in the p-type third layer, sample #42.

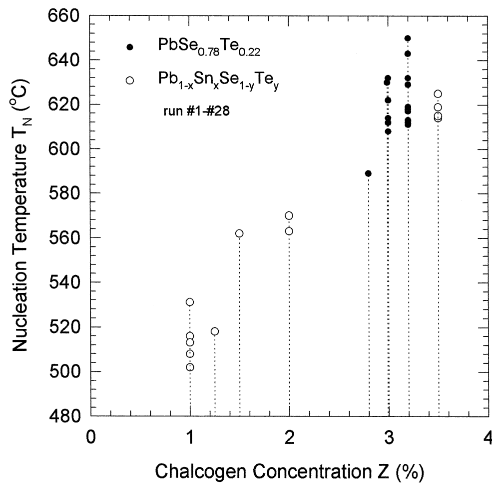

Fig. 4. Nucleation temperature vs. chalcogen concentration for low purity PbSe source material. Note the wide scatter of T_N from 611°C to 650°C at $z = 3.20\%$ for the ternary layers and from 502°C to 531°C at $z = 1.00\%$ for the quaternary layers.

was added to the growth solution for growing a p-type alloy. Pb, Sn, PbTe, and PbSe were weighed according to known lattice-matching conditions (primarily determined by Te content, y) for BaF_2 and desired nucleation temperatures (primarily determined by chalcogen content, z) of the growth solutions. A detailed procedure for cleaning lead and weighing the solid ingredients is described elsewhere [18]. The nucleation temperature (T_N) was measured for each liquid growth solution to determine the correct growth initiation temperature which was usually one or 2° above T_N. For a multiple-layer growth z was chosen so that the growth solution for growing each subsequent layer nucleated at a progressively lower temperature than the previous one. A heterostructure whose layers are grown at a progressively lower temperature is expected to have

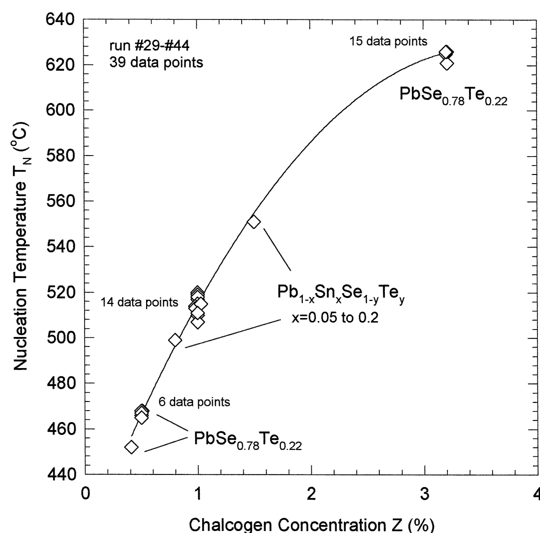

Fig. 5. Nucleation temperature vs. chalcogen concentration for high purity PbSe source material. Note the consistency of the T_N for a given z.

reduced interdiffusion at the heterojunctions. Typical growth parameters for a double heterostructure are listed in Table 1.

Nucleation temperature is defined as the temperature at which the onset of crystallization on the surface of the cooled liquid is visualized under a magnifying lens. It turned out that the nucleation temperature was highly sensitive to the purity of lead selenide sources in the growth solution. PbSe with 99.999% purity from CERAC, Milwaukee, WI was used for the first 28 growth experiments. PbSe synthesized from 99.9995% pure Pb and 99.9999% pure Se from Crystal, Berlin, Germany was used for the remaining 16 growth experiments. All growth experiments using the less pure (five 9's) PbSe source in the growth solutions resulted in a wide scatter of T_N for a given z—as large as a 39° variation at $z = 3.2\%$, shown in Fig. 4. By contrast, growth solutions containing the purer PbSe source exhibited a consistently monotonic increase of T_N with z as expected [7], see Fig. 5.

6. Growth procedures and results

Each growth experiment began with loading a prepared BaF_2 substrate followed by loading the solid constituents of the source materials for each layer into the corresponding growth well. The LPE furnace was then sealed and vacuumed down to between 2 and 6 mTorr using a cryogenic sorption pump. The furnace was then back filled and flushed with purified hydrogen prior to commencement of the growth sequence as well as during growth.

During the course of the study the previously used LPE growth procedure was modified several times leading to the development of an optimized three-stage growth procedure. In this procedure, growth solutions were loaded into consecutive wells starting from the first well for a multilayer growth experiment. Trapping of chalcogen vapor around BaF_2 was facilitated due to filled wells adjacent to the first well. To further secure the vapor trapping all unloaded wells can be filled with, for example, graphite blocks in future experiments. In the first stage the furnace was heated to a high temperature where solid sources begin to rapidly dissolve in the lead-rich solution. In stage two growth solutions were slowly cooled at a controlled rate of 2° min^{-1} until the nucleation temperature was recorded for each growth solution. In stage three the layer-by-layer growths took place over the same controlled cooling ramp as used in stage two. In this stage the substrate was pulled under the growth solution at the growth initiation temperature. Growth was allowed to continue while the furnace cooled for a specific length of time until it was terminated by pulling the substrate away from the well containing the growth solution. The growth time was counted from the time when the leading edge of the substrate entered the growth well to when the trailing edge left the well. All seven triple-layer double heterostructures were grown using the optimized growth procedure with the

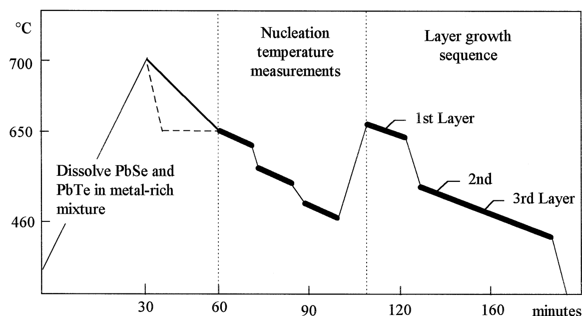

Fig. 6. Schematic representation of the growth sequence used for growing seven good IV–VI semiconductor triple-layer structures. In five (#39, #40, #41, #42, and #44) growth experiments the furnace was cooled normally (solid line) following dissolution of solid PbSe and PbTe in stage I. In two (#38 and #43) growth experiments, the furnace was held at a stable temperature (~ 25°C above the nucleation temperature of the first growth solution) for a 30-min growth solution homogenization (dashed line). The 2°C min^{-1} cooling ramp (thick lines) is employed during stages II and III for nucleation temperature measurements and layer growths, respectively. Normal fast cooling was allowed between the first and the second layer growths in order to bridge the 100° difference in growth initiation temperatures of the two layers.

growth sequence shown in Fig. 6. The new growth procedure took less than 240 min (196 min being the shortest), allowing the preparation and growth of a double heterostructure to be completed within an 8-h workday.

Table 2 shows the structures obtained from the 44 experiments in this study. Continuous epitaxial layers were obtained at growth initiation temperatures of 610°C to 652°C for the first layer (PbSeTe and PbSnSeTe), 508 C to 553°C for the second layer (PbSnSeTe with up to 20% tin in the liquid), and 453°C to 469°C for the third layer (PbSeTe). The PbSnSeTe alloy with 40% tin in the three *n*-PbSnSeTe/*n*-PbSeTe heterostructures grown at 504°C, 520°C, and 572°C showed epitaxial but discontinuous growths. The lack of continuous growth in these epilayers was attributed to the high tin content.

Not all growth experiments prior to the last seven triple-layer growths resulted in continuous epitaxial layers and/or fair wipeoffs. Factors contributing to poor growth results include scratches on the BaF_2 growth surface, over-etching of BaF_2, excessive substrate clearance, protrusion of substrate above the slider surface, separation of boat halves during slider pulling, and high tin content.

Two additional factors came into consideration which concerned the flatness of the BaF_2 growth surface and the homogeneity of the growth solution during wipeoff. Since BaF_2 slabs were hand polished using mechanical tools the thickness was usually uneven and the four clearance measurements on a BaF_2 growth surface were different. For the first 37 growth experiments, the substrates were placed in the pocket in random fashion with respect to the measured clearances. Out of the 37 experiments, the 36th run produced the best layers in addition to an excellent wipeoff. All four clearance measurements at the BaF_2 growth surface used in run #36 were zero (an exception). Although the flat substrate growth surface played an important role in producing the good results, it is impractical if not impossible to obtain such flat surfaces using hand-polishing procedures.

During growth the growth solution becomes inhomogeneous because its periphery solidifies sooner than its interior. The wiping-off of the inhomogeneous growth solution from the growth surface involved disposing the residual melt from the growth well as the substrate was being

Table 2
IV–VI semiconductor heterostructures grown on (100) BaF_2 by LPE

Structure	No. of growths	Sn (%)
n-PbSeTe	7	–
n-PbSnSeTe	7	5
n-PbSnSeTe/*n*-PbSeTe	19	5, 40
p-PbSnSeTe/*n*-PbSnSeTe	1	5
p-PbSeTe/*n*-PbSnSeTe/*n*-PbSeTe	7	5, 6, 8, 10, 12, 20

The *p*-type layer is doped with thallium (Tl = 2.08–3.00%).

Table 3
Angles representing tilting of BaF_2 growth surface from the leading edge to the trailing edge for triple layer growth experiments

Run no.	38	39	40	41	42	43	44
Angle (°)	0.23	0.23	0.10	0.20	0.11	0.14	0.16

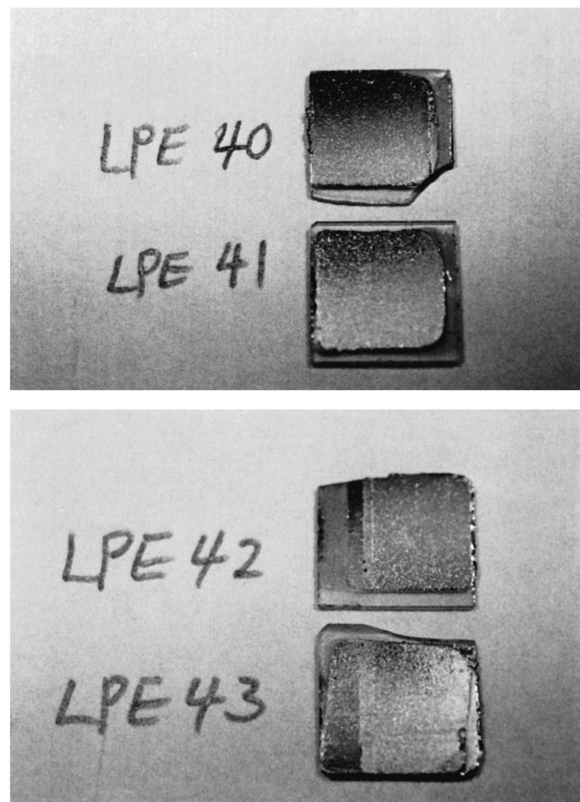

Fig. 7. Four samples showing LPE-grown IV–VI semiconductor PbSeTe/PbSnSeTe/PbSeTe double heterostructures on BaF_2 substrates. Parts of the first and the second layers can be seen on samples #42 and #43.

Table 4
Range of growth parameters used for triple-layer growths (#38–#44)

Epilayer	Lattice matching condition y (%)	Chalcogen content z (%)	Growth initiation temperature (°C)	Growth time (min)
1st	59.98–60.03	3.20–3.21	628	10
2nd	59.35–60.00	0.98–1.03	508–519	10
3rd	59.93–60.03	0.41–0.51	453–469	10–15

pulled away from the growth well. Depending on the location of the substrate pocket on the slider the residual melt either fell off the slider end onto the lower half of the boat or was swept off onto the slider. This presented two different situations where the surface tension, viscosity, and gravity determined the success of complete wipeoff. It turned out that very often a thin strip of solidified growth solution remained on the trailing edge of the grown layer regardless of the pocket location. However, the size of the melt adhesion could be large enough to resemble solidified volcano lava for experiments using pockets at the end of the slider (run #9 using the 20-mil pocket and run #21 using the 62-mil pocket).

Taking these two factors into consideration, a substrate orientation method was devised and used for the last seven growths. In this method BaF_2 was arranged so that the clearances at the trailing edge were greater than those at the leading edge. In other words, the largest slope (excluding the diagonal directions) of the BaF_2 growth surface is directed from the leading edge to the trailing edge. Using 40 μm as the maximum allowed clearance (or vertical drop) between the leading and the trailing edges, the corresponding surface slope would form a 0.23° angle with the slider surface. The actual angles for the last seven runs are listed in Table 3. These angles are very small and vary between 0.10° and 0.23°. If a flat growth surface is indeed crucial to growth solution wipeoff, these values reflect a window of flatness ($0° \leq \theta \leq 0.23°$) for obtaining good results. It is on these sloping growth surfaces that the three forces take place: the gravitational force acting on the lead-rich growth solution, the surface tension, and the viscosity of the partially and inhomogeneously solidified melt. All seven double-heterostructure growth experiments using the new substrate orienting method resulted in excellent wipeoffs. The epilayers of four double heterostructures are shown in Fig. 7.

Since consistent good layers and wipeoffs were obtained for the seven triple layer growth experiments conducted in like manner, a close examination of the techniques used for these growths is warranted. Common to these experiments are the following factors: (1) high purity (> 99.999%) PbSe source for growth solution; (2) properly polished and etched BaF_2 growth surface; (3) tight substrate clearance (within 40 μm); (4) 36-mil deep substrate pocket located away from slider end; (5) new substrate orientation method; (6) consecutive loading of wells; (7) locking device to secure boat closure during slider movement; (8) optimized triple-layer growth procedure. These factors which have been discussed previously are necessary ingredients in the recipe for good growths. The range of growth parameters used for the triple-layer growths is listed in Table 4. Note that within one structure, the

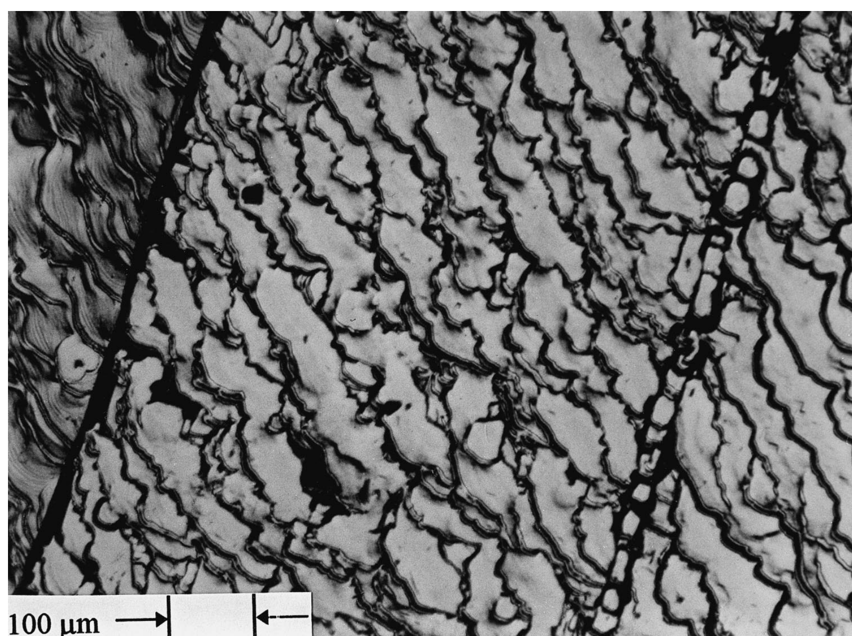

Fig. 8. Nomarski photograph showing surface morphology for the three epilayers in a PbSeTe/PbSnSeTe/PbSeTe double heterostructure (sample #42) grown by LPE. From left to right: first layer, second (quaternary) layer, and third layer.

largest span of growth initiation temperatures is 175° (#39) and the largest deviation of lattice matching parameter (y) is 0.68% (#40). These, together with Table 3 represents growth windows for a successful growth of a double heterostructure.

7. Surface morphology

The epilayers of the last seven growths are essentially inclusion-free when observed under optical microscopes with Nomarski interference. Fig. 8 shows a photograph of a typical surface morphology for a PbSeTe/PbSnSeTe/PbSeTe double heterostructure (sample #42) in which each of the three layers can be seen. The (100)-oriented terracing on each layer is typical of LPE-grown films on a slightly misoriented, i.e., not true (100) substrates. The smooth (100) facets are ten's of microns in width and can be as large as ~ 100 μm. Oriented cubic initial growth crystallites (not shown) are usually seen on bare BaF_2 around the edge of the epilayer.

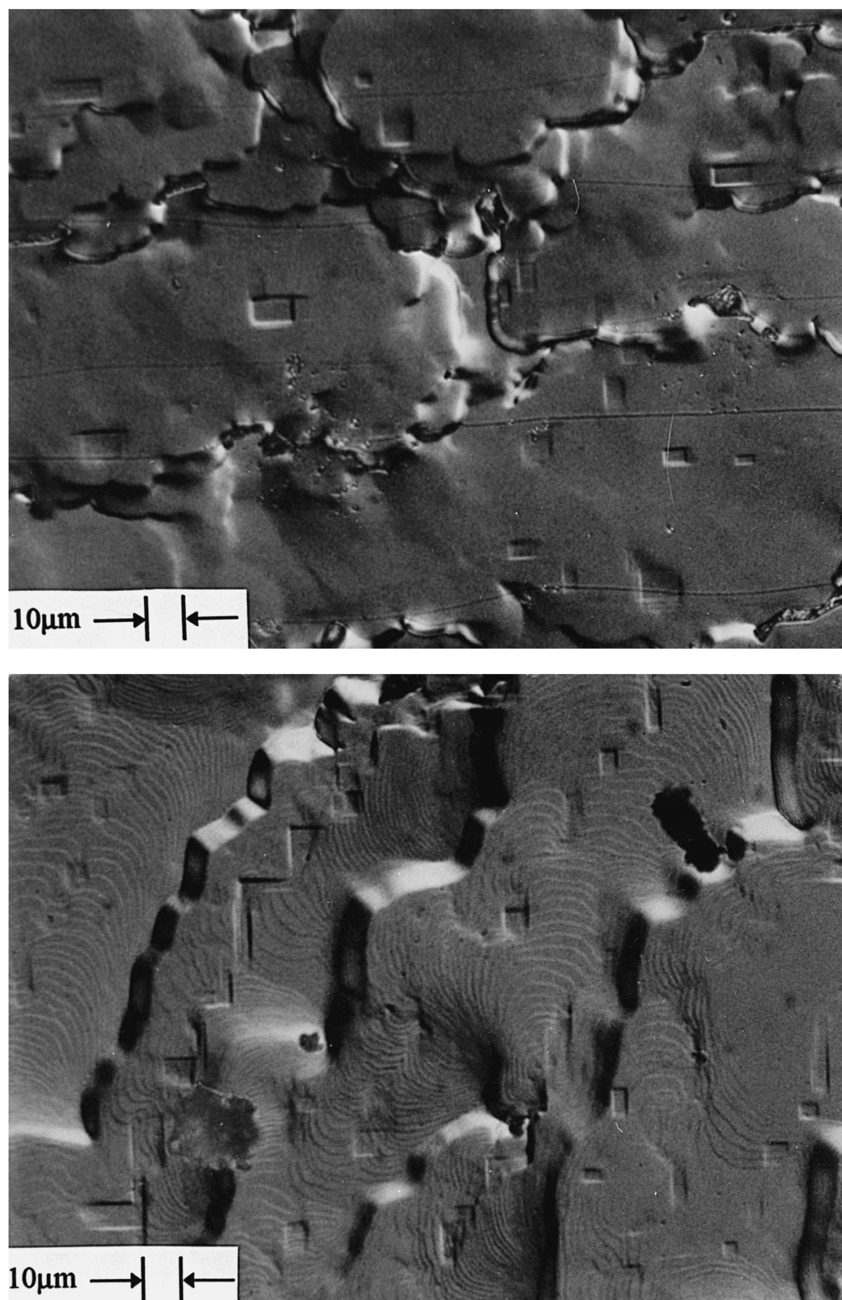

Fig. 9. Nomarski photograph of surface morphology of the p-PbSeTe layers of samples #40 (top) and #39 (bottom). These layers are the third layer of the PbSeTe/PbSnSeTe/PbSeTe double heterostructures grown by LPE.

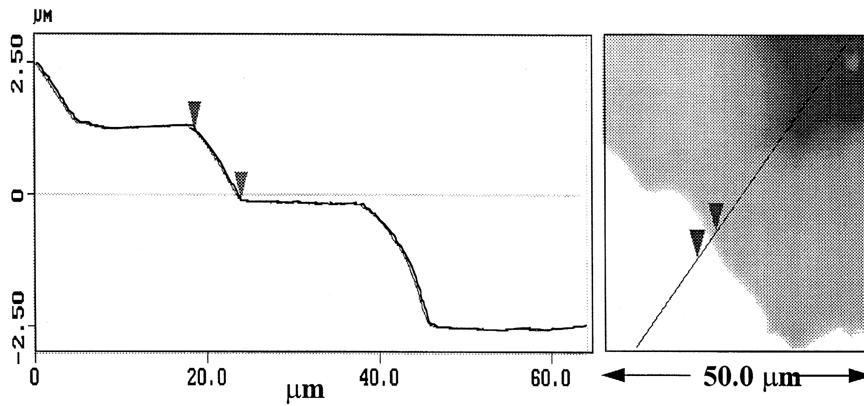

Fig. 10. AFM surface profile showing the depth of (100) growth facets on the p-PbSeTe top layer of a PbSeTe/PbSnSeTe/PbSeTe double heterostructure grown by LPE (sample #43). The step height of the facet indicated by the arrows are 1.5 μm.

Also observed is a new feature on all epilayers which appears as rectangular structures with micron-sized edges in the top layers of the double heterostructures (#39 and #40) (see Fig. 9). The scale of these structures is comparable to the finer terracing within each (100) faceted surface. The 'rectangles' are several to ten's of microns apart but can also be inter-connected as seen on sample #39. They occur randomly with varying density on each layer but the density is usually higher on the thallium-doped p-type top (third) layer than the native n-type first and second layers. They are oriented the same way as the initial growth crystallites. Some fine terracing and wipeoff lines are seen to run right on top of these structures. The formation mechanism of these structures is not well understood.

Surface morphology of the epilayers was further investigated using AFM, see Figs. 10 and 11. The sharp-rising ledge of the (100) facets ranges in height from 1/2 μm to 2 μm making the surface much rougher than IV–VI semiconductor layers grown by MBE. The 'rectangular structures' are actually shallow surface depressions with very gentle slopes. They are about 400 Å to 700 Å in depth at the lowest point relative to the top edge. They differ from etch pits which are usually more rounded when observed under an optical microscope and two orders of magnitude deeper.

8. Optical transmission measurements

The transmission of light through the samples was measured by a Bruker IR/98 FTIR spectrometer. Inside the optical bench radiation emitted by a graphite globar is directed through a KBr beam splitter and partially absorbed by the sample before reaching a HgCdTe detector having a peak detectivity at 16 μm. The radiation was normally incident on the back side of the sample through the BaF_2 substrate which is transparent up to 11 μm (912 cm^{-1}). Reference spectra were obtained from bare BaF_2 substrates and were used to ratio out the substrate effect. The bench is continuously vacuumed down to 15–20 mbar during measurements.

Room temperature transmission spectra for three different samples illustrating the effects of adding PbSeTe ternary cladding layers to a PbSnSeTe quaternary active layer with ~ 5% tin are shown in Fig. 12. In Fig. 12, the spectrum of

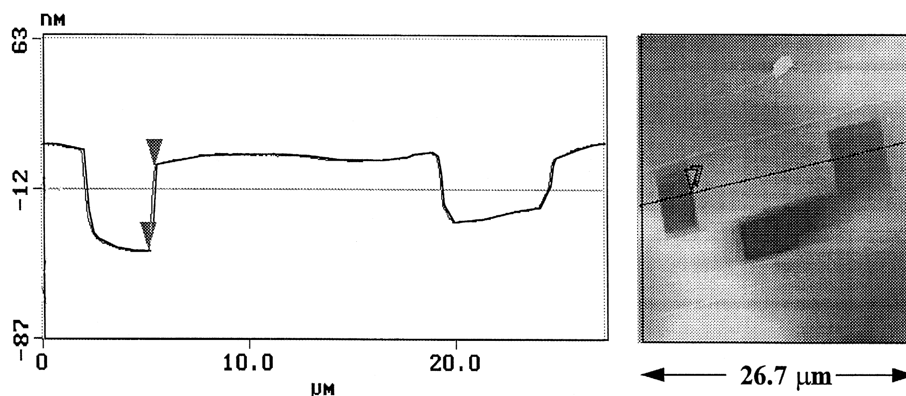

Fig. 11. AFM surface profile showing the submicron indention on the p-PbSeTe top layer of a PbSeTe/PbSnSeTe/PbSeTe double heterostructure grown by LPE (sample #40). Note that the length of the side indicated by the arrows is ~ 400 nm, forming a very shallow angle of ~ 6°.

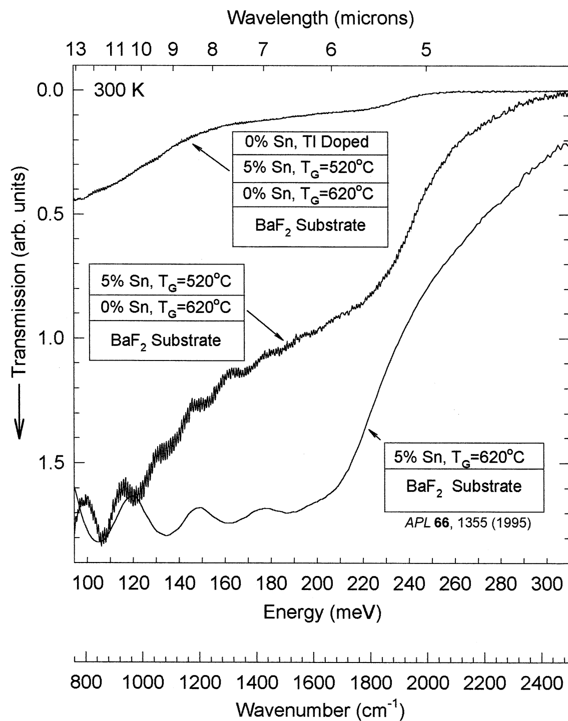

Fig. 12. FTIR transmission spectra for three different LPE-grown samples. The two-layer structure is ~7 μm thick and the single-layer structure is 2.2 μm thick [11].

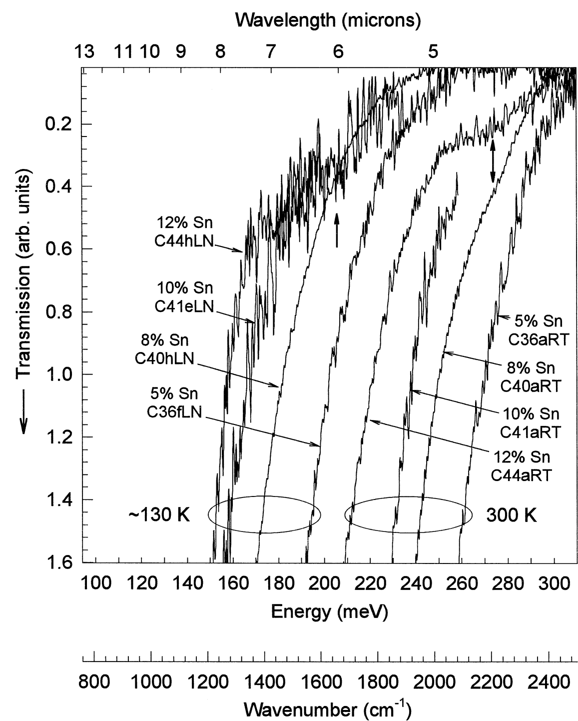

Fig. 13. FTIR transmission spectra for four LPE-grown heterostructures having different tin contents. Spectra, some of which are truncated for clarity, are grouped for measurements at 300 K and ~130 K. Absorption edges for the larger bandgap ternary cladding layers are marked with arrows.

a PbSnSeTe epilayer (bottom) obtained using another FTIR spectrometer [11] was compared to the spectra of a single heterostructure PbSnSeTe/PbSeTe (sample #36) and a double heterostructure PbSeTe/PbSnSeTe/PbSeTe (sample #38) grown in this study. The onset of absorption, which corresponds to the bandgap of the quaternary layer, shifts from ~200 meV for the single layer to 220 meV for the double- and triple-layer structures suggesting that less tin is incorporated in the quaternary layer when the growth temperature is reduced. (Preliminary photoluminescence experiments also show that quaternary layers grown at lower temperatures exhibit larger bandgaps, i.e., less tin.) A higher liquid-to-solid segregation coefficient for tin at higher growth temperatures is supported by the Pb–Sn–Se phase diagram [15]. Adding cladding layers to the quaternary layer also increases the total thickness of the film, resulting in increased free-carrier absorption. There appears to be an additional absorption edge at a lower energy (~100 meV) for the double- and triple-layer structures, a feature also seen on the spectra of other multilayer structures measured. IR absorption at energies below the bandgap in IV–VI semiconductors grown by different methods has been observed previously [19–22] but its origin is not yet well understood.

The Fabry–Perot interference fringes for the two-layer structure (sample #36) suggests a relatively uniform thickness of the LPE-grown structure. A Tensor step profile scan performed within 1 mm from the edge of the sample showed a typical thickness of 7 μm with variation between 6 μm and 8 μm. From the fringe spacing of the spectrum and the measured film thickness the average refractive index is calculated to be 5.1 at 11.7 μm. The much more tightly spaced fringes are due to interference caused by the BaF_2 substrate which is ~700 μm thick.

FTIR transmission spectra measured at two temperatures for four multilayer structures grown from solutions having different tin content (5%, 8%, 10%, and 12%) in the liquid growth solution for the quaternary layer are shown in Fig. 13. As expected, the absorption edge shifts to a lower energy as the tin content increases at both room

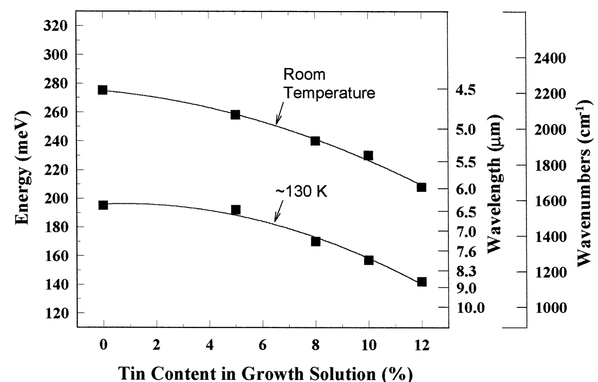

Fig. 14. Absorption edge energy of $Pb_{1-x}Sn_xSe_{1-y}Te_y$ alloys as a function of tin content in the liquid growth solution at two temperatures. Data points at 0% tin represent the absorption edge energy of the ternary cladding layer (sample #44).

temperature and ∼130 K. The absorption edge corresponding to the ternary cladding layers (marked by arrows) seen on some of the spectra also exhibits a similar temperature dependence. The effect of additional tin on the absorption edge at these two temperatures is more clearly seen in Fig. 14. This plot demonstrates that the bandgap energy of the quaternary alloy can be engineered independently by controlling the tin content and the sample heat sink temperature. The nonlinear behavior of the shift in absorption edge with tin content is also supported by the Pb–Sn–Se phase diagram [15], i.e., smaller liquid-to-solid segregation coefficient at higher tin content. Based on these data, change in bandgap energy is expected at an average rate of 0.41 meV per degree in the temperature range of 130 K to 300 K. The uniform shift in absorption edge with temperature suggests that the band discontinuity at the heterojunctions is preserved for structures having different tin content (5%–12%) in the quaternary layer. It also predicts stable tunability of the active quaternary layer in a given structure. These characteristics are important considerations in designing TDL devices. These structures show promise for fabricating TDL that span the spectra range of 4.8–6.6 μm (at 5% tin) and 6.0–8.7 μm (at 12% tin) in the temperature range measured.

9. Summary

IV–VI semiconductor single, double, and triple layer structures were grown latticed matched to (100) BaF_2 substrates from metal-rich PbSnSeTe growth solutions by LPE. Factors contributing to both poor and good growth results were discussed. PbSeTe/PbSnSeTe/PbSeTe double heterostructures with excellent growth quality and growth solution wipeoffs were consistently grown using a new growth procedure. Successful epitaxy of the second layer (active region for a double heterostructure laser) can be achieved at a growth initiation temperature as low as 508°C for tin contents up to 20%. Epilayers were characterized using Nomarski microscopy, AFM and FTIR spectroscopy. Surface morphology exhibits typical (100)-oriented growth facets and (100) faceted sub-micron features. Results of IR transmission measurements show that the absorption edge energies vary monotonically with tin content and with temperature at average rate of 0.41 meV per degree. TDL fabricated from these structures are expected to span a spectral range of 5 μm to 8 μm from 300 K to 130 K.

Acknowledgements

This work was supported by grants from the National Science Foundation (DMR-9416871) and the National Aeronautics and Space Administration Earth System Science Fellowship Program (NGT-30308).

References

[1] Z. Feit, J. Fuchs, D. Kostyk, W. Jalenak, Liquid phase epitaxy-grown PbSnSeTe/PbSe double heterostructure diode lasers, Infrared Phys. Tech. 37 (1996) 439.
[2] M. Loewenstein, Diode laser harmonic spectroscopy applied to in situ measurements of atmospheric trace molecules, J. Quant. Spectrosc. Radiat. Transfer 40 (1988) 249.
[3] P.S. Lee, R.M. Schreck, B.A. Hare, J.J. McGrath, Biomedical applications of tunable diode laser spectrometry, Ann. Biomed. Eng. 22 (1994) 120.
[4] Z. Feit, M. McDonald, R.J. Woods, V. Archambault, P. Mak, Low threshold PbEuSeTe/PbTe separate confinement buried heterostructure diode lasers, Appl. Phys. Lett. 68 (1996) 738.
[5] J. Faist, C. Gmachl, F. Capasso, C. Sirtori, D.L. Sivco, J.N. Baillargeon, A.Y. Cho, Distributed feedback quantum cascade lasers, Appl. Phys. Lett. 70 (1997) 2670.
[6] P.J. McCann, C.G. Fonstad, Liquid phase epitaxy growth of PbSe on (111) and (100) barium fluoride, J. Cryst. Growth 114 (1991) 687.
[7] P.J. McCann, C.G. Fonstad, Growth of $PbSe_{0.78}Te_{0.22}$ lattice matched with BaF_2, Thin Solid Films 227 (1993) 185.
[8] P.J. McCann, D. Zhong, Liquid phase epitaxy growth of $Pb_{1-x}Sn_xSe_{1-y}Te_y$ alloys lattice matched with BaF_2, J. Appl. Phys. 75 (1994) 1145.
[9] P.J. McCann, S. Aanegola, J.E. Furneaux, Growth and characterization of thallium and gold-doped $PbSe_{0.78}Te_{0.22}$ layers lattice matched with BaF_2 substrates, Appl. Phys. Lett. 65 (1994) 2185.
[10] I. Chao, S. Yuan, P.J. McCann, Growth and characterization of PbSeTe/PbSnSeTe/PbSeTe double heterostructures, Int. Semicond. Device Res. Symp. Proc. 2 (1996) 505.
[11] P.J. McCann, L. Li, J. Furneaux, R. Wright, Optical properties of ternary and quaternary IV–VI semiconductor layers on (100) BaF_2 substrates, Appl. Phys. Lett. 66 (1995) 1355.
[12] P.J. McCann, High temperature semiconductor lasers, US Patent #5,454,002, Issued September 26, 1995.
[13] P.J. McCann, K.R. Lewelling, Prospects for high operating temperature IV–VI semiconductor tunable diode lasers, Optical Remote Sensing for Environmental and Process Monitoring, Air and Waste Management Association, Pittsburgh, PA, 1996, p. 26.
[14] K.R. Lewelling, P.J. McCann, Finite element modeling predicts possibility of thermoelectrically cooled lead–salt diode lasers, IEEE Phot. Tech. Lett. 9 (1997) 297.
[15] P.J. McCann, J. Fuchs, Z. Feit, C.G. Fonstad, Phase equilibria and liquid phase epitaxy growth of PbSnSeTe lattice matched to PbSe, J. Appl. Phys. 62 (1987) 2994.
[16] P.J. McCann, C.G. Fonstad, Auger electron spectroscopic analysis of barium fluoride surfaces exposed to selenium vapor, J. Electron. Mater. 20 (1991) 915.
[17] P.J. McCann, S. Aanegola, The role of graphite boat design in liquid phase epitaxial growth of $PbSe_{0.78}Te_{0.22}$ on BaF_2, J. Cryst. Growth 141 (1994) 376.
[18] S. Aanegola, Liquid phase epitaxial growth of $PbSe_{0.78}Te_{0.22}$ layers lattice matched with BaF_2: graphite boat design and doping behavior, Master's Thesis, University of Oklahoma, 1994.
[19] H.R. Riedl, Free-carrier absorption in *p*-type PbTe, Phys. Rev. 127 (1962) 162.
[20] Y.B. Grekov, V.V. Prudnikov, N.A. Semikolenova, Investigation of the nature of additional long-wavelength absorption in $Pb_{1-x}Sn_xTe$, Sov. Phys. Semicond. 15 (1981) 1194.
[21] K.V. Kolezhuk, T.A. Kudydina, I.A. Samoilova, IR absorption spectra in $Pb_{0.83}Sn_{0.17}Te$, Infrared Phys. 25 (1985) 375.
[22] D.M. Zayachuk, V.I. Garasim, V.A. Shenderovskii, Self-compensation and deep levels in $Pb_{1-x}Sn_xS_{1-y}Se_y$ crystals, Mater. Sci. Eng. B 14 (1992) 398.